

Structural Characterisation of Hierarchically Porous Silica Monolith by NMR Cryo-porometry and -diffusometry

Seungtaik Hwang^{1*}, Rustem Valiullin¹, Jürgen Haase¹, Bernd M. Smarsly²,
Armin Bunde², Jörg Kärger¹

¹ Universität Leipzig, Fakultät für Physik und Geowissenschaften, Germany

² Justus-Liebig-Universität Gießen, Institute of Physical Chemistry, Germany

Corresponding author: Seungtaik Hwang, Fakultät für Physik und Geowissenschaften,
Universität Leipzig, Linnèstr. 5, 04103 Leipzig, Germany, E-Mail:
seungtaik.hwang@physik.uni-leipzig.de

Abstract

A systematic NMR cryo-porometry and -diffusometry study using nitrobenzene as a probe liquid is carried out in order to characterise pore structures of hierarchically-organised porous silica monolith possessing mesopores along with a 3D bicontinuous macropore network. The result obtained from NMR cryoporometry shows the presence of a relatively wide mesopore size distribution of 10-35 nm. Furthermore, NMR cryodiffusometry indicates that whilst the mesopores are highly tortuous ($\tau_{\text{meso}} \approx 6$), they have little influence on the overall tortuosity of the material ($\tau_{\text{overall}} \approx 1.5$), which is largely dominated by the macropores ($\tau_{\text{macro}} \approx 1.7$).

Keywords

NMR cryoporometry, pore size distribution (PSD), PFG NMR, NMR cryodiffusometry, hierarchically porous silica monolith

1. Introduction

Due to enormous practical importance of nanostructured porous materials in diverse fields, such as catalysis and gas separations, there has been a constant demand for novel experimental techniques for probing pore-structural properties of such materials in a well-defined way. Amongst many experimental techniques, nuclear magnetic resonance (NMR) has been considered as a powerful tool yielding valuable information on pore space in porous materials [1-4]. In particular, textural and structural properties, for example, pore size distribution (PSD) and tortuosity factor, τ , of porous materials can be effectively measured by employing NMR techniques at low temperatures, i.e. NMR cryo-porometry and -diffusometry [5-7]. In the present work, a systematic study of NMR is carried out at low temperatures in order to characterise different pore spaces in hierarchically porous silica monolith possessing mesopores

along with a 3D bicontinuous macropore network. This experimental approach has enabled us not only to suppress the NMR signal from solid phase with an appropriate interpulse delay, but also to confine the diffusion of intrapore fluid exclusively into mesopores by freezing out the fluid in macropores. As a result, we can simultaneously monitor phase equilibrium of the intrapore fluid and its diffusion in each pore space. Nitrobenzene is used as a probe liquid since it exhibits a sharp bulk phase transition between liquid and solid phases at a relatively mild temperature of 5.7 °C. Such conditions are of use, especially when plotting a melting curve of the guest molecules confined in a porous medium with a wide pore size distribution. The data of nitrobenzene melting curves are converted to PSD using the Gibbs-Thomson equation. With NMR cryodiffusometry we measure the effective long-range diffusivities of nitrobenzene confined in different pores and calculate the tortuosity factor of each pore space, which exhibits valuable information on the inter pore connectivity.

2. Methods and Materials

2.1. Hierarchically Porous Silica Monolith

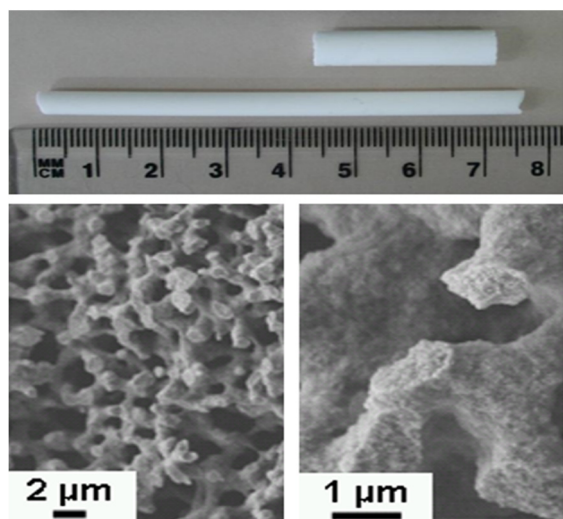


Figure 1. Photograph and SEM images of hierarchically porous silica monolith with mesopore and a 3D bicontinuous macropore network [10].

The porous silica monoliths produced by the Nakanishi process [8-9] were prepared in the Smarsly lab [10]. In the present work, two types of silica monoliths were used: one is silica monolith with macropores (ca. 2-4 μm) only, and the other, which is shown in Fig 1., is hierarchically porous silica monolith possessing both macro- and mesopores. For sample preparation, the monoliths were broken into small grains or fine powders and outgassed using a vacuum pump. Then, they were soaked in nitrobenzene for at least 24 hours under ambient conditions to fully saturate the pores. Whilst the powder sample was placed in an NMR tube with excess nitrobenzene, the samples with small grains were prepared without excess liquid on the external surface.

2.2. NMR Cryoporometry

NMR cryoporometry exploits the difference in the transverse NMR relaxation rates between solid and liquid phases. With an interpulse delay of 3 ms between the radiofrequency pulses in the Hahn echo pulse sequence, the NMR signal from the solid phase was effectively suppressed, so that the signal from the liquid phase could be measured exclusively [4]. Therefore, the normalised signal intensity was proportional to the number of nitrobenzene molecules in the liquid phase in the pores. A complete melting curve was plotted by the following procedure: firstly, temperature was slowly decreased until the nitrobenzene was completely frozen out and the spin-echo signal disappeared. The signal disappeared at a very low temperature which is far lower than the bulk equilibrium transition temperature due to a strong supercooling effect. Secondly, the temperature was increased in small steps, giving 500 s to reach phase equilibrium after every temperature increment. Then, the spin-echo signal was measured at each temperature. After plotting a melting curve of nitrobenzene confined in the pores, the detected

temperature shift of melting point of nitrobenzene was used to produce the pore size distribution (PSD), according to the Gibbs-Thomson equation:

$$\Delta T_m(d_p) = T_0 - T_m = K_{GT}/d_p \quad \text{Eq. 1}$$

where d_p is pore diameter, T_0 is bulk equilibrium transition temperature, T_m is actual melting point, and K_{GT} is Gibbs-Thomson coefficient for the liquid in the pores.

2.3. NMR Cryodiffusometry

Pulsed field gradient (PFG) NMR experiments with Hahn echo pulse or 13-interval sequence [11] were conducted on a home-built spectrometer operating at 125 MHz for protons to measure the effective, long-range diffusivities of the supercooled nitrobenzene at 0 °C along the freezing branch. The basic concept of this NMR cryodiffusometry is to trace the diffusion behaviour of the probe liquid confined in a specific pore subpopulation which is set and controlled by freezing or melting the liquid [4, 12]. To measure its diffusivity solely in the mesopores, the macropores should be blocked and only the mesopores are open. This condition was achieved by slowly heating the frozen sample up to a temperature slightly below T_0 (5.7 °C for nitrobenzene) and reversing the direction of the temperature change, i.e. from melting branch to freezing branch, to drop it down to 0 °C. In this way, the presence of a seed crystal or nucleus which initiated the crystal homogeneous nucleation cancelled out the undesired supercooling effect; hence nitrobenzene in the macropores and bulk nitrobenzene on the external surface were completely frozen at 0 °C (see Fig. 2 Sample A). On the other hand, nitrobenzene confined in the mesopores remained in the liquid phase since such confinement led to a depression in the freezing (or melting) point which was inversely proportional to the pore size, i.e. the Gibbs-Thomson effect [4]. Fig 2. shows the samples under study. The calculated diffusivities were used to determine the tortuosity factors of different pore spaces according to the following equation:

$$\tau = D_{\text{bulk}} / D_{\text{pore}} \quad \text{Eq. 2}$$

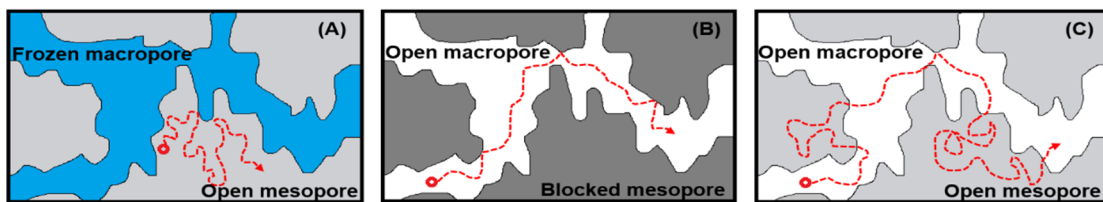


Figure 2. Samples with different pore spaces. (A) a nitrobenzene molecule diffusing exclusively in the mesopores. The macropores are blocked due to the frozen phase of nitrobenzene there. (B) a nitrobenzene molecule diffusing exclusively in the macropores. No mesopores are present in this material. (C) a nitrobenzene molecule diffusing through the hierarchically porous silica monolith with both meso- and macropores.

3. Results and Discussion

Upon heating the samples up, starting from a completely frozen state of nitrobenzene, the spin-echo signal intensities corresponding to the number of nitrobenzene molecules in the liquid phase in the pores were recorded to plot the so-called melting curves shown in Fig. 3. The signal from the solid phase was effectively eliminated using an interpulse delay of 3 ms between the two radiofrequency pulses in the Hahn echo pulse sequence since the transverse relaxation

times in the frozen nitrobenzene phase were sufficiently shorter than 3 ms. As expected, a sharp bulk phase transition between liquid and solid phases was observed at around 5.7 °C for all the samples.

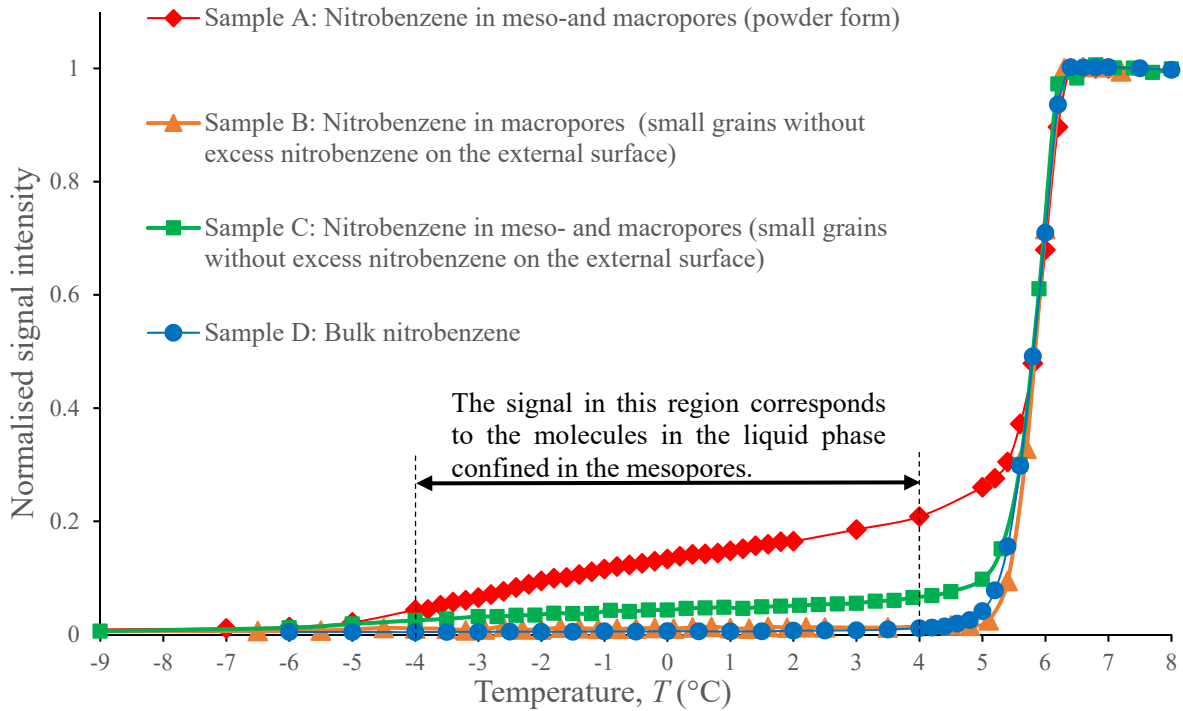


Figure 3. Melting curves of nitrobenzene in different samples. (A) Nitrobenzene in meso- and macropores (powder form). (B) Nitrobenzene in macropores (small grains without excess nitrobenzene on the external surface). (C) Nitrobenzene in meso- and macropores (small grains without excess nitrobenzene on the external surface). (D) Bulk nitrobenzene

For samples A and C in Fig. 3, there is a gradual increase of the signal intensity in the region between $T = -4$ °C and $T = 4$ °C. The signal intensity in this region represents the number of the molecules in the liquid phase confined in the mesopores, and hence their corresponding volume, V_p . The gradual increase, therefore, implies the presence of a wide distribution of the mesopore sizes as well as a high interpore connectivity. If the samples had a well-defined mesopore structure with unconnected linear pores, we would have observed a sharp stepwise increase of the signal intensity in the region, as shown by Kondrashova et al. [13].

The collected data of Fig. 3 can be readily converted to the pore size distribution (PSD) function presented in Fig. 4 using the literature value of the Gibbs-Thomson coefficient for nitrobenzene, $K_{GT} = 125$ K nm [4] and the Strange-Rahman-Smith equation [14, 15]:

$$\frac{dV_p}{dd_p} = \frac{dV_p}{dT} \frac{K_{GT}}{d_p^2} \quad \text{Eq. 3}$$

where V_p is pore volume, d_p is pore diameter, T is temperature, and K_{GT} is Gibbs-Thomson coefficient for the liquid in the pores.

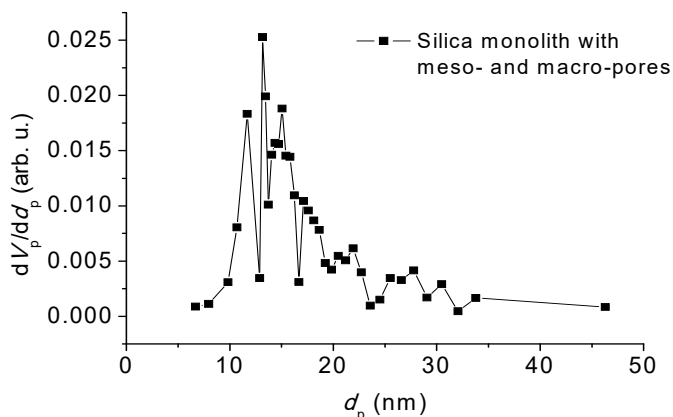


Figure 4. Pore size distribution of the hierarchically porous silica monolith with meso- and macropores, obtained from NMR cryoporometry. The solid line serves as a guide to the eye.

The details of the relevant calculations can be found elsewhere [12, 13]. The obtained PSD in Fig. 4 shows the highest peak at around $d_p=13$ nm. As we predicted from the gradual increase of the signal intensity in Fig. 3, the PSD exhibits a relatively wide mesopore size distribution of 10-35 nm.

In addition to NMR cryoporometry, PFG NMR experiments were conducted at 0 °C (along the freezing branch) using four different observation times, t , i.e. different diffusion times. In the measurements, the 13-interval sequence was employed for 10, 40 and 160 ms. However, for the shorter observation time of 2 ms, the Hahn echo pulse sequence was used since it was too short for the 13-interval sequence in which a finite duration of the z-storage delay was required. The obtained spin-echo attenuation plots for $t = 40$ ms are only presented in Fig. 5, as an example. Shown are the first linear parts of the spin-echo attenuations yielding the effective (mean) diffusivities in the pores [16].

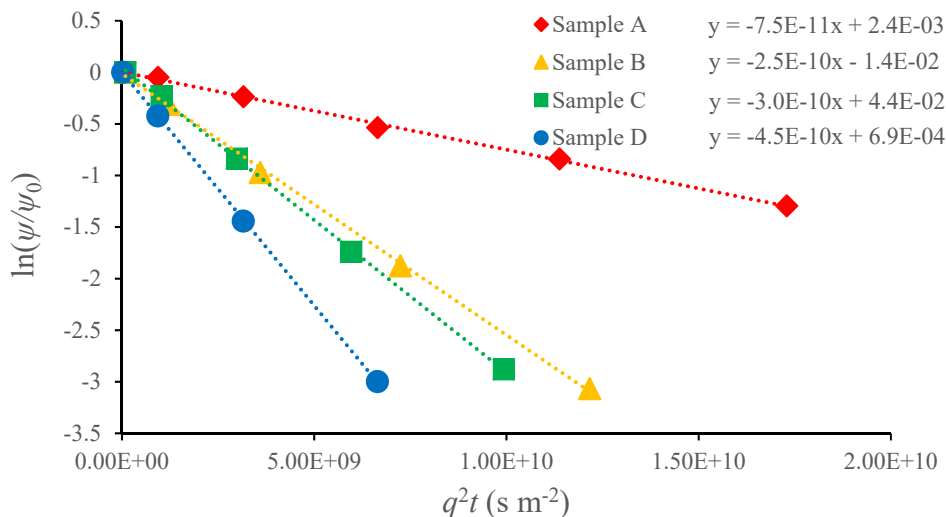


Figure 5. Spin-echo attenuation plots for $t = 40$ ms. (A) Solely mesopores. (B) Solely macropores. (C) Both meso- and macropores. (D) Bulk nitrobenzene

Fig. 6 (a) and (b) show the final results of the NMR cryodiffusometry experiments performed with the four samples. Using nitrobenzene as a probe liquid, the diffusivities have already reached a plateau even at $t = 2$ ms, thereby yielding the long-range diffusion only. It is because the displacement of the slowest Sample A during the given observation times already far exceeds the size of the mesopores (see Fig. 6 (b)). Another probe liquid with a lower diffusivity is needed to further study the short-range diffusion and the transient regime.

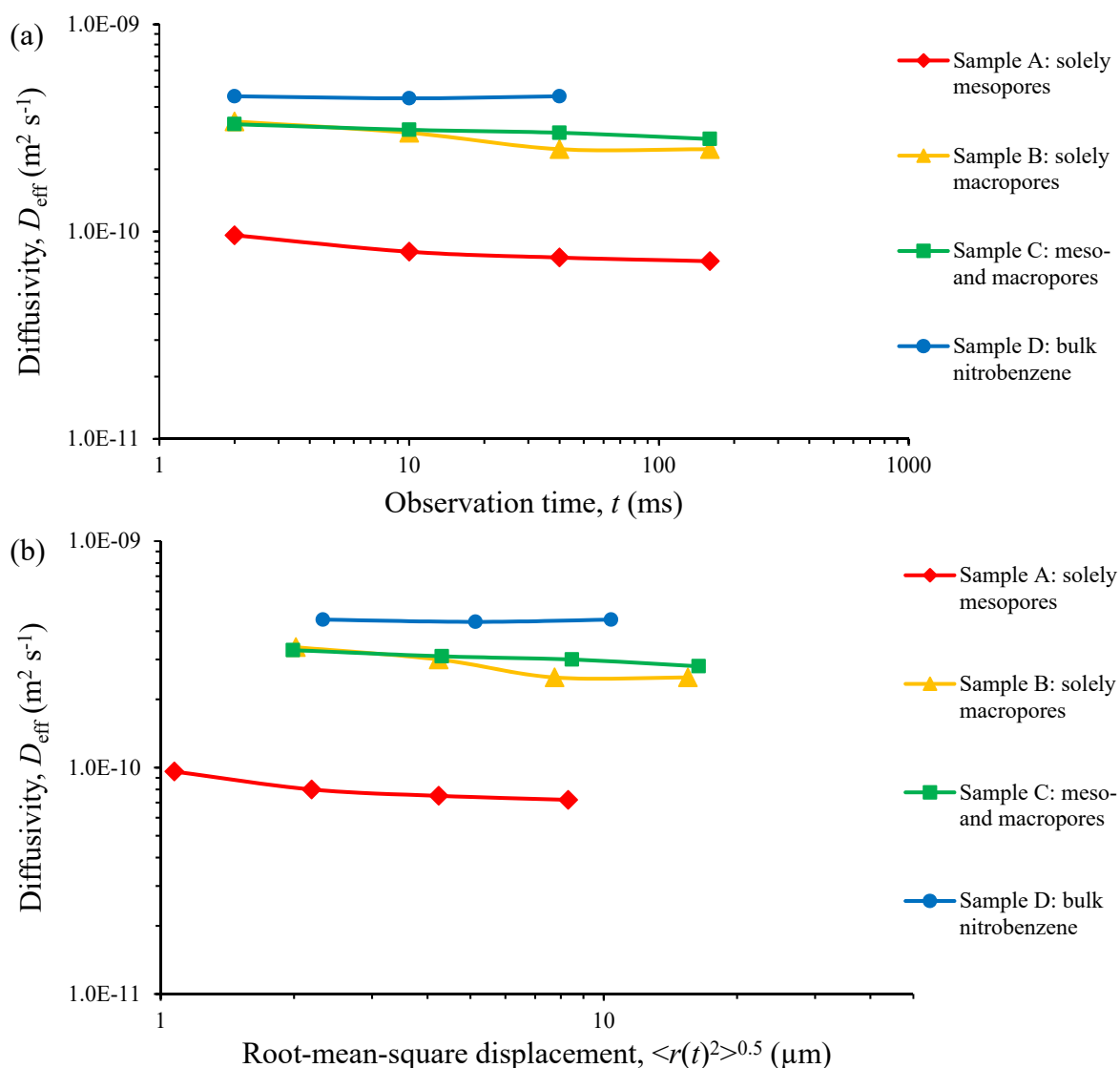


Figure 6. Diffusivities for nitrobenzene as a function of observation time (a) and root-mean-square displacement (b)

The calculated diffusivities can be used to estimate the tortuosity factors of different pore space using Eq. 2. The tortuosity factor of the mesopores is then defined as $\tau_{\text{meso}} = D_{\text{bulk}} / D_{\text{eff,meso}}$, which is approximately 6. Similarly, $\tau_{\text{macro}} = D_{\text{bulk}} / D_{\text{eff,macro}} \approx 1.7$ and $\tau_{\text{overall}} = D_{\text{bulk}} / D_{\text{eff,overall}} \approx 1.5$. Whilst the mesopores are highly tortuous, they have little influence on the overall tortuosity of the material, which is largely dominated by the macropores.

4. Conclusions

In the present work, a systematic study of nuclear magnetic resonance (NMR) at low temperatures using nitrobenzene as a probe liquid is carried out. We demonstrate and discuss the applicability of our experimental approach in probing pore-structural properties, such as pore size distribution (PSD) and tortuosity factor, of a specific subpopulation of pores

separately even in hierarchically porous silica monolith in which meso- and macropores coexist and are well-connected. It is shown that the experimental method, intentionally freezing and melting the intrapore fluid, can be successfully used to effectively eliminate the spin-echo signal from the solid phase and to continuously monitor the phase equilibrium of the fluid and its diffusion in each subpopulation of the pores in other hierarchically porous materials.

The PSD obtained from the NMR cryoporometry indicates the presence of a wide mesopore size distribution of 10-35 nm in the hierarchically porous silica monolith. In the NMR cryodiffusometry, we estimate the diffusivities of nitrobenzene in different pore spaces and their tortuosity factors. The mesopores in the silica monolith are much more tortuous than the macropores. Since the root-mean-square displacement of nitrobenzene far exceeds the size of the mesopore, further research using another probe liquid with a lower diffusivity is necessary to understand the short-range diffusion and the transient regime.

Acknowledgement

Financial support by the DFG (BU 534/22, KA953/30 and HA1893/17-1) is gratefully acknowledged.

References

- [1] A.T. Watson and C.T.P. Chang, *Prog. Nucl. Magn. Reson. Spectrosc.*, 31 (1997) 343.
- [2] F. Stallmach and J. Kärger, *J. Int. Adsorpt. Soc.*, 5 (1999) 117.
- [3] Y.Q. Song, H. Cho, T. Hopper, A.E. Pomerantz and P.Z. Sun, *J. Chem., Phys.*, 128 (2008) 052212.
- [4] D. Kondrashova, M. Dvoyashkin and R. Valiullin, *New J. Phys.*, 13 (2011) 015008.
- [5] A.V. Filippov and V.D. Skirda, *Colloid J.*, 63 (2000) 759–764.
- [6] E.L. Perkins, J.P. Lowe, K.J. Edler, N. Tanko and S.P. Rigby, *Chem. Eng. Sci.*, 68 (2008) 1929–1940.
- [7] P.A.C. Gane, C.J. Ridgway, E. Lehtinen, R. Valiullin, I. Furò, J. Schoelkopf, H. Paulapuro and J. Daicic, *Ind. Eng. Chem. Res.*, 43 (2004) 7920–7927.
- [8] K. Nakanishi and N. Soga, *J. Am. Ceram. Soc.*, 74 (1991) 2518.
- [9] K. Nakanishi and N. Soga, *J. Non-Cryst. Solids.*, 139 (1992) 1.
- [10] Y. Hu, P. Adelhelm, B.M. Smarsly, S. Hore, M. Antonietti and J. Maier, *Adv. Funct. Mater.*, 17 (2007) 1873-1878.
- [11] P. Galvosas, F. Stallmach and J. Kärger, *J. Magn. Reson.*, 166 (2004) 164–173.
- [12] J. Beau and W. Weber, *Prog. Nucl. Magn. Reson. Spectrosc.*, 56 (2010) 78–93.
- [13] D. Kondrashova and R. Valiullin, *J. Phys. Chem. C*, 119 (2015) 4312–4323.
- [14] J.H. Strange, M. Rahman and E.G. Smith, *Phys. Rev. Lett.*, 71 (1993) 2589.
- [15] J. Mitchell, J. Beau, W. Webber and J.H. Strange, *Phys. Rep.* 461 (2008) 1–36.
- [16] R. Valiullin, M. Dvoyashkin, P. Kortunov, C. Krause and J. Kärger, *J. Chem. Phys.* 126 (2007) 054705.